NANO · MICRO small
www.small-journal.com

Ion/Electron Redistributed 3D Flexible Host for Achieving Highly Reversible Li Metal Batteries

Huai Jiang, Yangen Zhou, Caohong Guan, Maohui Bai, Furong Qin, Maoyi Yi, Jie Li, Bo Hong, and Yanqing Lai**

3D carbon frameworks are promising hosts to achieve highly reversible lithium (Li) metal anodes, whereas insufficient effects are attributed to their single electron conductivity causing local aggregating of electron/Li^+ and uncontrollable Li dendrites. Herein, an ion/electron redistributed 3D flexible host is designed by lithiophilic carbon fiber cloth (CFC) modified with metal–organic framework (MOF)-derived porous carbon sheath with embedded CoP nanoparticles (CoP-C@CFC). Theory calculations demonstrate the strong binding energy and plenty of charge transfer from the reaction between CoP and Li atom are presented, which is beneficial to in situ construct a Li_3P@Co ion/electron conductive interface on every single CoP-C@CFC. Thanks to the high ionic conductive Li_3P and electron-conductive Co nanoparticles, the rapid dispersion of Li^+ and obviously reduced local current density can be achieved simultaneously. Furthermore, in situ optical microscopy observations display obvious depression for volume expansion and Li dendrites. As expected, a miraculous average Coulombic efficiency (CE) of 99.96% over 1100 cycles at 3 mA cm^{-2} and a low overpotential of 11.5 mV with prolonged cycling of over 3200 h at 20% depth of discharge are successfully obtained. Consequently, the CoP-C@CFC-Li||$LiFePO_4$ full cells maintain a capacity retention of 95.8% with high CE of 99.96% over 500 cycles at 2 C and excellent rate capability.

1. Introduction

The ambitious goal of being carbon neutral all over the world will strongly drive the electrification of the automobile, so that more efficient energy storage systems are urgently needed.[1,2] Comparing to current Li-ion batteries consisting of graphite anode (350–400 Wh kg^{-1}), Li metal batteries matched with Li metal anodes exhibit an irresistible attraction due to high energy densities (3500 Wh kg^{-1} in Li–air battery, and 2600 Wh kg^{-1} in Li–S battery).[3,4] However, poor cycling reversibility and potential safety hazards from Li dendrite growth limit its practical application, which are ascribed primarily to non-uniform Li deposition and huge volume effect.[5] To overstride these obstructions, considerable efforts have been devoted, including tailoring new electrolytes and additives to in situ form robust solid electrolyte interphase (SEI) layers,[6,7] constructing solid state electrolytes to hinder Li dendrites,[8,9] regulating appropriate external factors (temperature,[10] pressure,[11] or current density[12]), designing novel 3D Li metal,[13,14] and ingenious porous metal current collectors.[15,16] Although Li dendrites could be partially suppressed via these strategies, highly reversible Li plating/stripping is still difficult to realize effectively under realistic current density with high capacity.

Fortunately, the 3D carbon frameworks with large specific area not only decrease local current density and inhibit Li dendrite growth, but also depress huge volume expansion, contributing to achieve highly reversible Li metal anodes with high energy density.[17] Thus, all kinds of novel 3D carbon matrixes, such as carbon fibers,[18,19] 3D graphene-based skeletons,[20] and hollow carbon sphere,[21] have been verified. Among them, benefitting from the excellent mechanical property, free-standing, low-cost, and easy to large-scale production, carbon fiber cloth (CFC) displays an enormous practical potential as a high-performance host of Li metal anode.[22,23] However, as-fabricated 3D carbon frameworks are mostly single electron-conductive skeletons, which induces inhomogeneous electron accumulation and then drives Li^+ non-uniform distribution or transfer on the surface of CFC as shown in **Figure 1**a. It leads to dendritic Li accumulating on the surface of electrode with most of the 3D void being not fully utilized.[24–26] Despite lithiophilicity modification with precious or transition metal (Au,[27] Ni,[28] Ag[29]), transition metal oxides (ZnO,[30] RuO_2,[31] NiO[32]), metal sulfides (Cu_7S_4),[33] and metallic nitrides (Ni_xN[34]) inducing Li selective deposition could partially settle these problems, this

H. Jiang, Y. Zhou, M. Bai, F. Qin, M. Yi, J. Li, B. Hong, Y. Lai
School of Metallurgy and Environment
Central South University
Changsha, Hunan 410083, China
E-mail: bop_hong@csu.edu.cn; laiyanqing@csu.edu.cn
C. Guan
University of Michigan–Shanghai Jiao Tong University Joint Institute
Shanghai Jiao Tong University
800 Dongchuan Road, Shanghai 200240, China
B. Hong, Y. Lai
Engineering Research Centre of Advanced Battery Materials
The Ministry of Education
Changsha, Hunan 410083, China
The ORCID identification number(s) for the author(s) of this article can be found under https://doi.org/10.1002/smll.202107641.

DOI: 10.1002/smll.202107641

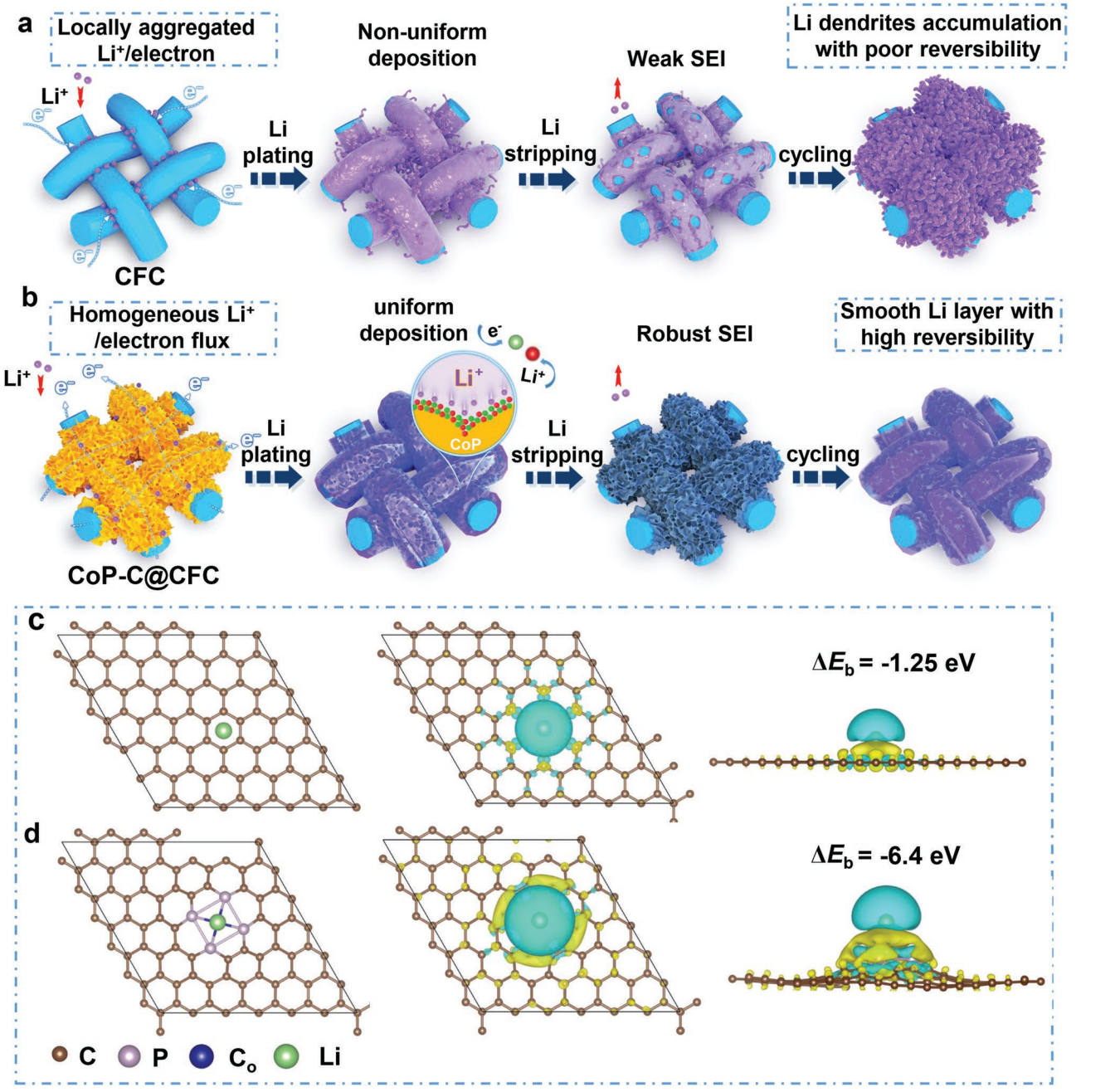

Figure 1. Li plating/stripping process on a) CFC and b) CoP-C@CFC electrode. Binding energies of a Li atom with c) CFC and d) CoP-C@CFC at the top sites by density functional theory calculations.

phenomenon of ion/electron maldistribution is hard to change in essence. Besides, lithiophilic materials with these disadvantages of high cost and easy to structural failure hinder its commercial application. Recently, MOF derivates with weak conductivity acting as inert sheath in situ enfold the CFC core to low local current density and change uneven charge distribution of electrode interface.[35,36] Furthermore, abundant lithiophilic sites as nucleation seeds guide Li uniform deposition.[37,38] However, owing to the single electron-conductive carbon skeleton and the as-formed insulated Li_2O product, the polarization of battery increase significantly, which usually is harmful for uniform Li plating/stripping.[39,40] To fundamentally settle the problem of ion/electron uneven distribution on 3D carbon fibers, there is still an urgent demand to explore a high-efficiency carbon fiber host with superior structural stability, lithiophilicity, and 3D mixed ion/electron conductivity.

Here, we construct a MOF-derived porous carbon sheath with embedded CoP nanoparticles-modified CFC (CoP-C@CFC) (Figure 1b), whose electrode interface is further transferred to Co particles surrounded by Li_3P networks through the lithiation of CoP nanoparticles, in situ forming a 3D mixed ion/electron conductive interface for interfacial charge and Li^+

redistribution. Importantly, the CoP-C@CFC shows multiple findings: 1) weakly conductive MOF-derived porous carbon sheath is regarded as insulated "outerwear," which weakens space charge polarization of pure CFC (Figure 1a) and uniforms Li^+/electron flux into entire 3D skeletons; 2) density functional theory (DFT) calculations demonstrate stronger binding energy from the reaction between CoP and Li atom (−6.4 eV) and a plenty of charge transfer as shown in Figure 1c,d, thus driving the forming of Li_3P@Co ion/electron conductive interface; 3) the fast ionic conductive Li_3P (10^{-4} S cm^{-1}) and electron-conductive Co nanoparticles homogenize the Li^+ flux and charge distribution on the surface of CoP-C@CFC during the repeated Li plating/stripping (Figure 1b); 4) the lithiophilic CoP and reversible Li_3P product effectively eliminate nucleation barriers and form robust SEI layer, which are helpful to achieve permanent Li affinity and smooth Li layer with high reversibility; 5) a strong and flexible carbon scaffold to suffer huge pressure fluctuations and depress volume effect. Therefore, the well-designed carbon fiber skeletons achieve an amazing high average Coulombic efficiency (CE) of 99.96% with a sustainable lifespan of 1100 cycles at practical current density of 3 mA cm^{-2}. Moreover, the symmetric batteries with limited CoP-C@CFC-Li composite anodes also present a very low overpotential of 11.5 mV over 3200 h at 1 mA cm^{-2} with 1 mAh cm^{-2} (20% depth of discharge [DOD]). Coupled with $LiFePO_4$ (LFP) cathode, the CoP-C@CFC-Li‖LFP full cells hold a capacity retention of 95.8% with 130 mAh g^{-1} over 500 cycles at 2 C and excellent rate capability. Based on these advantages, CoP-C@CFC is an extremely promising candidate for high specific capacity, large-scale, and high-performance Li metal anodes.

2. Results and Discussion

As shown in **Figure 2**a, CoP-C@CFC was fabricated by a scalable room-temperature crystallization and annealing-phosphating process.[41,42] In brief, Co-MOF (ZIF-67) nanoflakes arrays were in situ grown onto the CFC via a facile solution crystallization method using mixing a given amount of $Co(NO_3)_2 \cdot 6H_2O$ and 2-methylimidazole (2-Melm) in aqueous solution at room temperature. 2D Co-MOF nanoflakes arrays uniformly covered on the smooth surface of pure CFC wiped off by acid solution (Figure 2b). As depicted in Figure 2c, plenty of the regular Co-MOF nanoflakes arrays grow vertically on the CFC (Co-MOF@CFC), which is just like beautiful hydrangea. Subsequently, the Co-MOF precursor was annealed in Ar and air atmosphere successively, during which the organic ligands were chemically transformed into porous carbon sheath and Co_3O_4 nanoparticles (Figure S1, Supporting Information) were evenly anchored (Co_3O_4-C@CFC). Then, the Co_3O_4-C@CFC is further transformed into CoP-C@CFC through low temperature phosphating under Ar atmosphere. Eventually, smooth carbon fibers skeletons were uniformly covered by interlaced CoP nanoflakes with abundant microporosity (Figure 2d), whose thickness is about 4.8 μm (Figure S2, Supporting Information) indicating compact and steady 3D composite carbon frameworks. Phase changes are also reflected in the color of the CFC. The gray pure CFC turns to purple and black successively (Figure S3, Supporting Information), which is owed to the composited Co-MOF precursor and porous carbon sheath with embedded CoP nanoparticles (CoP-C), respectively. Additionally, inappropriate solution concentration and soaking time affect the in situ growth of Co-MOF nanoflakes on the CFC (Figure S4, Supporting Information), which subsequently forms undesired CoP embedded carbon nanosheets (Figure S5, Supporting Information) and falls to fabricate CoP sheath. From EDX spectrograms (Figure S7, Supporting Information) and element mapping images (Figure 2e), the matched spatial distributions of C, P, and Co elements are exhibited, which further confirms the uniform coating of CoP-C on CFC skeleton. CoP nanoparticles with a particle size of about 15 nm could be found uniformly embedded in the carbon nanosheets (Figure S6, Supporting Information). High-resolution TEM characterization reveals unambiguous lattice fringe with the spacing of 0.187 nm, corresponding to the (202) plane of CoP (Figure 2f). Furthermore, the legible diffraction ring is showed in the selected area electron diffraction pattern, which further testifies the high crystallinity of CoP (Figure 2g).

The phase structures of CFC, Co-MOF@CFC, and CoP-C@CFC are further confirmed by the Xray diffraction (XRD) patterns in **Figure 3**a. There are two clear broad peaks at about 24.5° and 43.8° shown in XRD result of CFC, which indicates poor crystallization. Co-MOF in situ grows onto the CFC, whose phase is tested by the comparison of the XRD results between Co-MOF@CFC and simulated Co-MOF. After annealing-phosphating process, CoP-C@CFC is successfully achieved with obvious characteristic peaks of CoP. CoP-C@CFC also presents high specific surface area of 60.517 m^2 g^{-1} from the results of Brunauer–Emmett–Teller test (Figure 3b), which is 23 times as much as CFC. It indicates that MOF-derived porous carbon sheath with embedded CoP nanoparticles effectively enhance specific surface area of carbon fiber skeletons, which is beneficial to higher Li capacity and lower local current density. In addition, the pore size distribution displays plenty of micropores/mesopores of ≈20 nm originated from porous carbon sheath with embedded CoP nanoparticles, which provides abundant Li nucleation interface and loading space of Li metal (Figure S8, Supporting Information). The surface chemical composition and status of CoP-C@CFC are further investigated by X-ray photoelectron spectroscopy (XPS). As shown in Figure S9, Supporting Information, the characteristic peaks of C, O, Co, and P are clearly presented, indicating these elements co-existence. In Figure 3c, two clear characteristic peaks located at 778.0 and 781.1 eV are indexed to Co $2p_{3/2}$. Another strong peak located at 796.9 eV corresponds to Co $2p_{1/2}$. The peaks at 778.0 and 796.9 eV are close to the binding energies of Co into CoP.[43]

Additionally, owing to the shake-up excitation of the high-spin Co^{2+}, the satellite peaks are observed at 783.4, 787.0, 798.4, 801.7, and 804.2 eV. In Figure 3d, the characteristic peaks of P $2p_{1/2}$ and P $2p_{3/2}$ are situated at 131.1 and 129.7 eV, which relate to Co-P.[44] The clear species of the P-O compound is confirmed by the strong peak of 134.1 eV, which is attributed to oxidation.

To preliminarily testify the lithiophilicity of CoP-C@CFC, binding energy (E_b) of a Li atom with CoP in CoP-C@CFC or pure CFC is estimated by DFT calculations. As shown in Figure 1c, Li atom adsorbs on the optimal structure of pure carbon, which displays the calculated binding energy (ΔE_b)

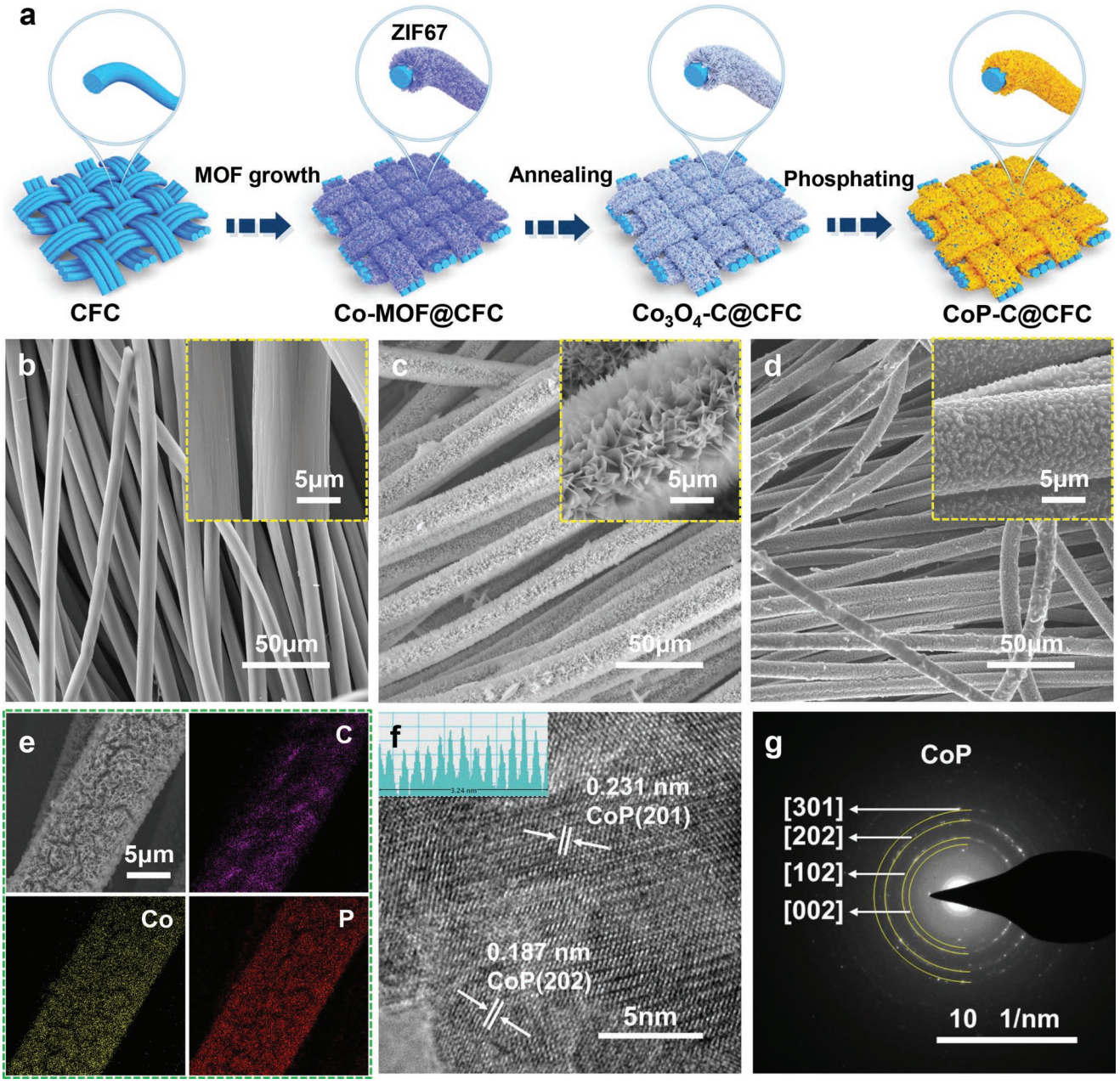

Figure 2. a) Schematic of the preparation process of CoP-C@CFC. SEM images of b) CFC, c) Co-MOF@CFC, and d) CoP-C@CFC. e) Elemental mapping of C, P, and Co elements in a single CoP-C@CFC. f) HRTEM and g) SAED of the CoP-C@CFC.

of −1.25 eV. Comparatively, the calculated binding energy of Li atom (T sites) with the optimal structure of CoP is −6.4 eV (Figure 1d), which is higher than ΔE_b of Li atom at H sites (Figure S10, Supporting Information) indicating superior Li affinity relative to pure carbon. Compared to CoP-C@CFC, Co_3O_4-C@CFC presents the lower ΔE_b of −4.62 eV and higher nucleation overpotential of 9 mV (Figure S11, Supporting Information), which elucidates the better lithiophilicity of CoP-C@CFC. In addition, the electron accumulation and depletion between Li with pure CFC or CoP-C@CFC also are shown in Figure 1c,d. In the 3D mode of Li atom adsorption, the yellow and light blue regions represent electron reduction and accumulation, respectively. Compared with pure carbon, amount of charge spontaneously transfers from Li atom to CoP-C@CFC substrate, which reveals stronger bond capability between Li and CoP-C@CFC. To intuitively verify lithiophilicity of CoP-C@CFC host, the wettability test of molten Li infusing CFC and CoP-C@CFC are performed. As shown in **Figure 4**a, the CFC substrate have not been wetted obviously in 90 s and displays poor lithiophilicity, owing to the "lithiophobic" nature of pure carbon. By contrast, CoP-C@CFC host contacts the molten Li to exhibit prominent Li affinity, whose disk center is rapidly infused liquid Li (Figure 4b). After 10 s, the molten Li has permeated carbon fibers layer presenting silvery character.

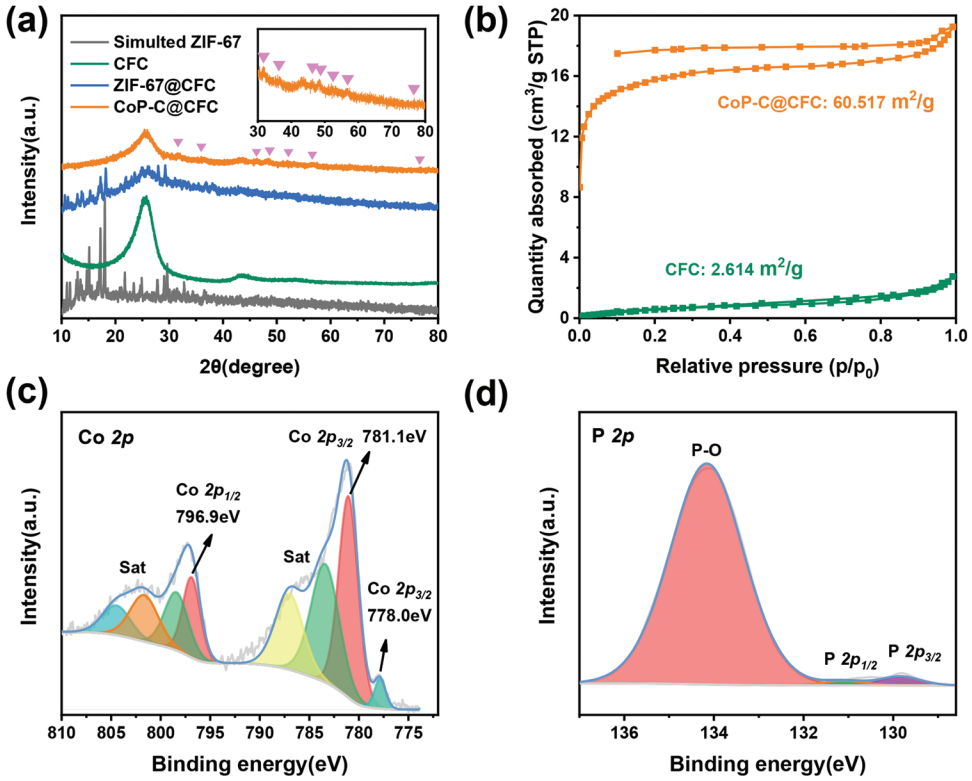

Figure 3. Characterization of CoP-C@CFC. a) XRD patterns of CFC, Co-MOF@CFC, and CoP-C@CFC. b) N_2 adsorption–desorption isotherm curve of CoP-C@CFC. c) Co 2p and d) P 2p XPS spectra of CoP-C@CFC.

Liquid Li metal continues along with every single carbon fiber to diffuse in 30 seconds (Figure S12a, Supporting Information), which displays contact angle of zero between Li metal and CoP-C@CFC substrate. Finally, Li metal uniformly spreads out entire surface of CoP-C@CFC electrode (Figure S12b, Supporting Information) and has successfully blended with each other after 90 s, while little Li metal attach on the surface of CFC. Therefore, the above theoretic calculations and wettability results demonstrate that CoP-C@CFC has outstanding lithiophilicity, which will benefit homogeneous Li nucleation and deposition along the surface of the carbon fibers due to the more favorable energy. To further study the nature of lithiophilicity, electrodeposition is performed to fabricate the 3D composite Li metal anode of CoP-C@CFC-Li, whose component is further characterized with XRD and XPS. The peaks of well-crystallized Co phase are clearly found in XRD pattern, while the peak of Li_3P is not obviously detected due to the low crystallization (Figure 4c). To deeply verify the formation of Li_3P phase, high-resolution XPS spectra of Li 1s is introduced in Figure 4d. Obviously, the peaks located at 56.9 eV are assigned to the generation of Li-P bonds,[25,45] and Li_3P phase turns to be the dominant components for fast Li^+ distribution (Figure 4d).[46] Correspondingly, the cyclic voltammetry (CV) curves of CoP-C@CFC within the potential ranging from 3.0 to 0.01 V in initial five cycles are presented in Figure 4e. In the first cathodic scan, the peak at 1.75 V is attributed to the lithiation of carbon–oxygen functional groups.[47] When the voltage drops at 1.4 V, the appearance of a broad irreversible reduction peak could owe to a transition phase of Li_xCoP formed by the lithium intercalation of the CoP.[48] With the scan voltage below 1 V, the successive slope can be related to the continuous transformation to Co and Li_3P accompanying with some irreversible reactions related with the SEI film.[49] In the first cycle of the oxidation process, the Li_3P is delithiated corresponding to the peak located at 1.1 V. After the first cycle, due to the structural reconstruction of the active material, the broad cathodic peak in the range 1.75–0.5 V shifts to 2.0 and 0.6 V during the following cycles, which corresponds to the formation of Li_xCoP and Li_3P. This is a common phenomenon for the conversion-type anode materials. The anodic peak at 1.1 V is assignable to the reversible reaction to CoP.[43] The following CV curves are stable and reproducible, indicating a good reversibility of CoP-C@CFC. Thus, the reaction mechanism has be revealed: 1) $CoP + xLi^+ + xe^- \leftrightarrow Li_xCoP$; 2) $Li_xCoP + (3-x)\ Li^+ + (3-x)\ e^- \leftrightarrow Li_3P + Co$. Benefitting from constructed ion/electron conductive interface of Li_3P@Co on the CoP-C@CFC electrode,[24,25,50] outstanding Li affinity and Li^+ diffusion kinetics could be achieved simultaneously. Moreover, CoP-C@CFC electrode displays the nucleation overpotential of 7.4 mV (Figure S13, Supporting Information), which is obvious lower than CFC electrode (23.3 mV).

To further understand the effect of CoP-C@CFC on Li deposition behavior, the morphology evolutions of Li plating on Li foil, CFC, and CoP-C@CFC electrode were studied by in situ and ex situ technologies. As depicted in **Figure 5**b, Li prefers to uneven nucleation and deposition on the interface of separator/CFC electrode due to inhomogeneous pristine carbon fibers (Figure 5a), causing much dendritic Li to form. When

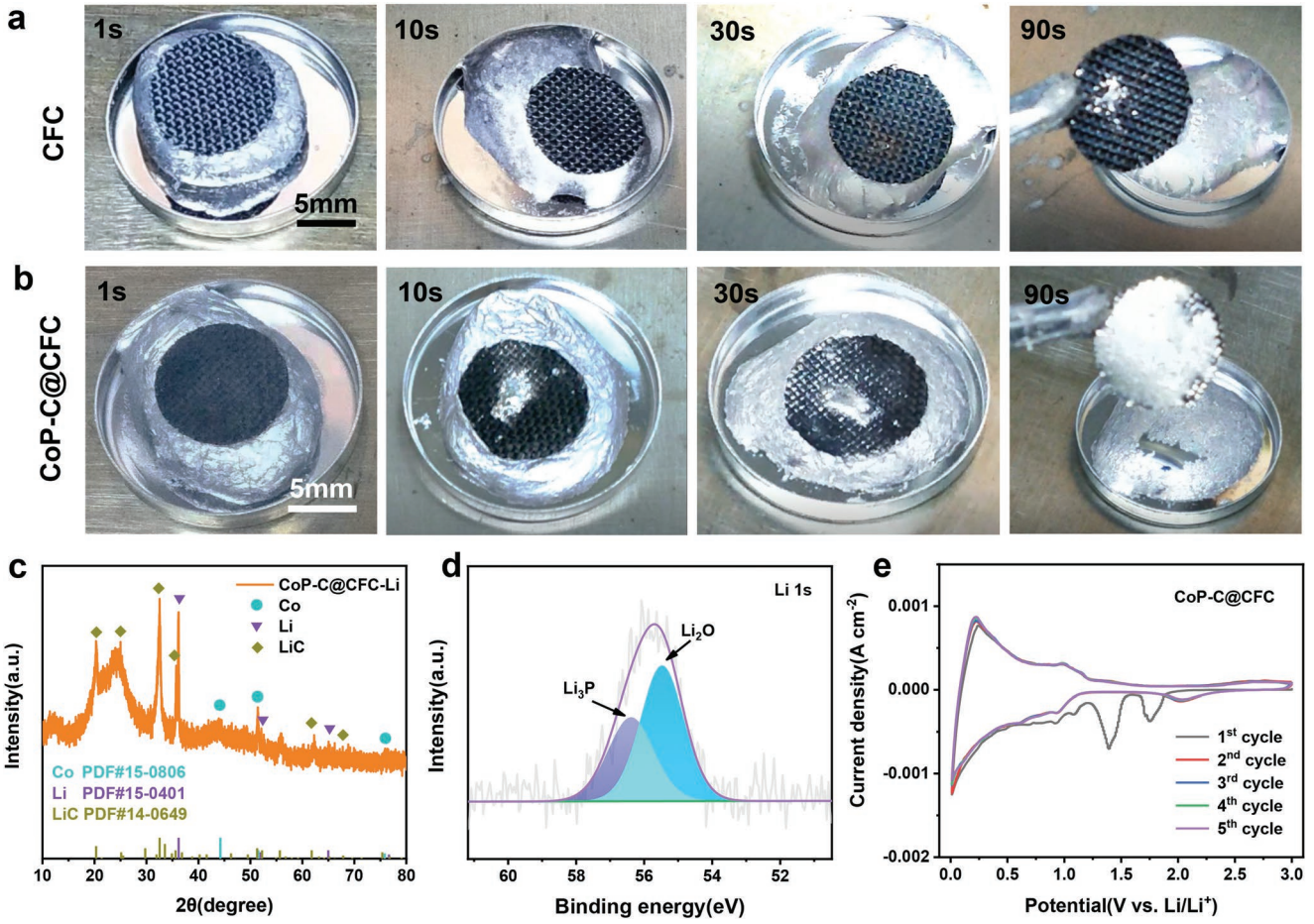

Figure 4. The lithiophilicity test of CoP-C@CFC. Wettability comparison of molten Li onto a) CFC and b) CoP-C@CFC substrates. c) The reaction product of CoP-C@CFC and Li metal. d) High-resolution XPS spectra of Li 1s to study the interfacial composition of CoP-C@CFC-Li. e) The cyclic voltammogram of CoP-C@CFC during the initial five cycles from 3.0 to 0.01 V.

the Li deposition capacity is raised to 5 mAh cm^{-2}, moss-like Li dendrites overspread the entire CFC electrode (Figure 5c). With the capacity further increasing to 10 mAh cm^{-2}, a mass of Li dendrites accumulates on the surface of CFC leading to the plugging of pore space (Figure 5d). Comparatively, Li uniformly plates on every single carbon fiber modified with MOF-derived porous carbon sheath with embedded CoP nanoparticles (Figure 5e), which displays dendrite-free Li deposition in Figure 5f. When the Li metal of 5 mAh cm^{-2} is deposited, the diameter of every single CoP-C@CFC becomes significantly larger due to evenly covered Li metal layer. Despite the capacity of 10 mAh cm^{-2} is further executed, Li metal still uniformly spreads over whole 3D carbon frameworks without dendritic Li accumulating. From the cross section of the electrode, the diameter of every single CoP-C@CFC obviously increases in varying degrees after deposited with the capacity of 2 or 5 mAh cm^{-2} compared with pristine (Figure S14a–c, Supporting Information). When the deposition capacity is raised to 10 mAh cm^{-2} (Figure S14d, Supporting Information), homogeneous Li metal fills with the gap of CFC without Li dendrites (Figure S15, Supporting Information). Furthermore, the thickness of the electrode has no obvious change (Figure S14e-h, Supporting Information). It indicates that CoP-C@CFC host possesses markedly superior Li affinity and the regulating capability of Li deposition. To deeply explore Li growth behavior and volume effect on CoP-C@CFC electrode, in situ optical microscopy is used to record the dynamic process of Li deposition. Initially, the capacity of 10 mAh cm^{-2} is predeposited in CFC and CoP-C@CFC, which is used to assembled symmetric cells. For pure Li foil, we can see a relative flat surface and compact structure at 10 s (Figure 5i). However, as Li foil is plated from 10 to 30 min (Figure 5j–l), the surface of Li foil electrode becomes fleeciness accompanying with obvious Li dendrites in the red dotted circle. The thickness of Li foil is raised to 1.5 times relative to pristine after continuous plating of 30 min, which presents simultaneously huge volume effect. Similarly, conspicuous Li dendrites and volume change also occur in CFC-Li electrode, whose thickness is increased to near two times (Figure 5m–p). Compared with pure Li foil, Li dendrites on CFC electrode begin to form 10 min late (Figure 5o), which means CFC can delay the forming of Li dendrites due to large specific area and lower local current density. Distinctively, CoP-C@CFC-Li electrode exhibits ultrastable Li plating accompanying with dendrite-free alongside with almost no volume expansion throughout the whole process (Figure 5q–t). It indicates that MOF-derived porous carbon sheath with embedded

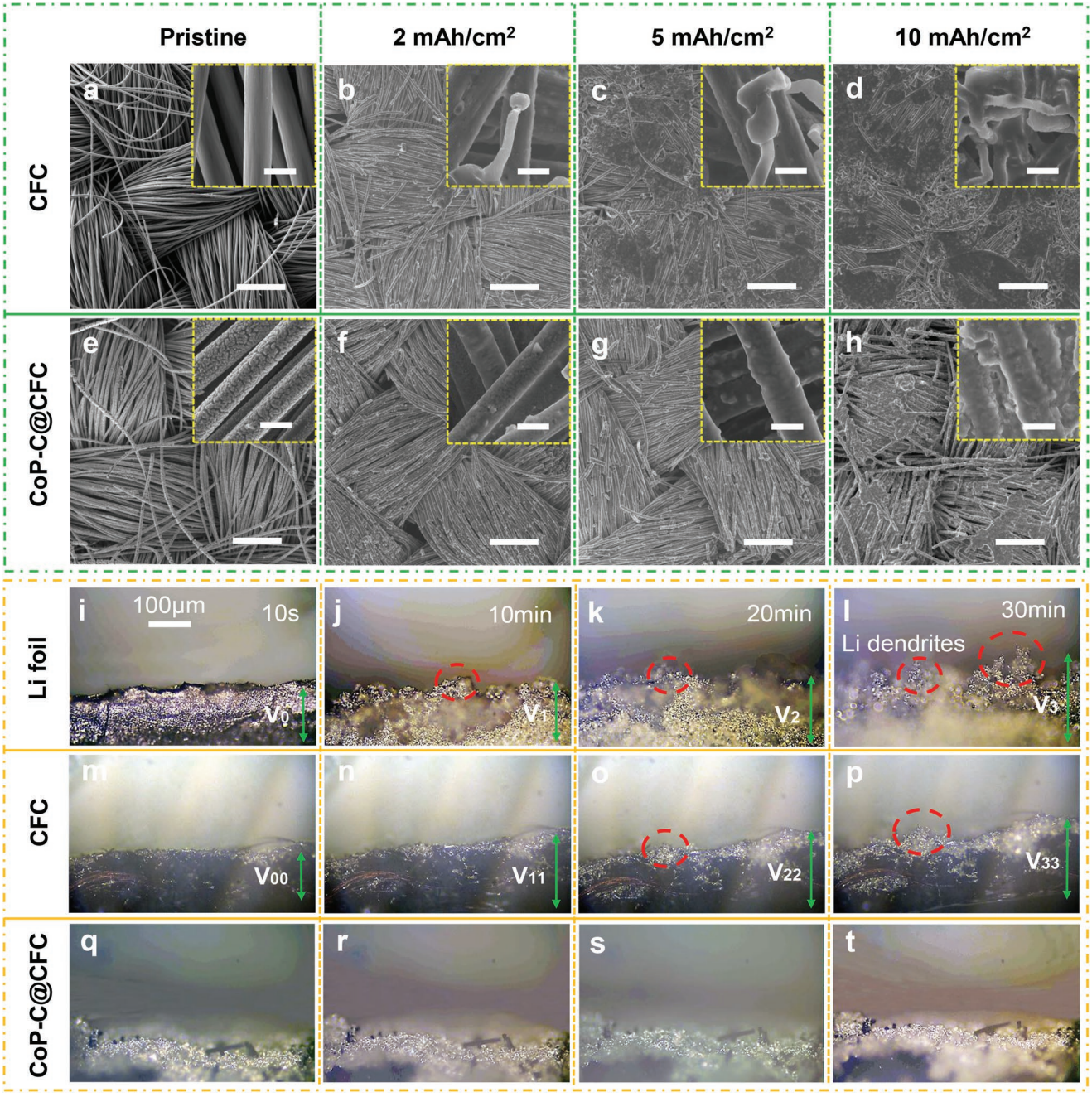

Figure 5. The morphologies of CFC and CoP-C@CFC electrode by plating Li metal with different capacity at 0.5 mA cm^{-2}. SEM images of a–d) CFC and e–h) CoP-C@CFC electrode with 0, 2, 5, and 10 mAh cm^{-2}, respectively. In situ optical microscopy observations of the Li deposition process with i–l) Li foil, m–p) CFC-Li, and q–t) CoP-C@CFC-Li as electrodes at 3 mA cm^{-2}. The scale bars are 10 μm in yellow dotted box, the others are 200 μm.

CoP nanoparticles guides uniform Li deposition, inhibiting Li dendrites and volume effect.

The electrochemical performance of CoP-C@CFC is evaluated by half-cell and symmetric-cell. As shown in **Figure 6**a, the CFC electrode displays a low average CE of 96.3% with rapidly terminative cycling lifespan at 3 mA cm^{-2} with the capacity of 1 mAh cm^{-2}, which possibly is caused by inhomogeneous Li deposition induced plenty of "dead" Li. When the capacity of Li deposition is raised to 2 mAh cm^{-2}, the CFC electrode can maintain relative stability, whereas the CE appears drop dramatically in 100 cycles due to Li dendrites accumulation leading to short circuit. Similarly, unstable CE and short cycling life are further deteriorated at 5 mA cm^{-2} with the capacity of 3 mAh cm^{-2}, which reveals poor electrochemical performance. By contrast, the CoP-C@CFC electrode shows an ultrastable average CE of 99.96% with ultralong cycle life of over 1100 cycles. Although the capacity of Li plating/stripping increases to 2 mAh cm^{-2}, a high average CE of 99.67% can still be maintained. Even at

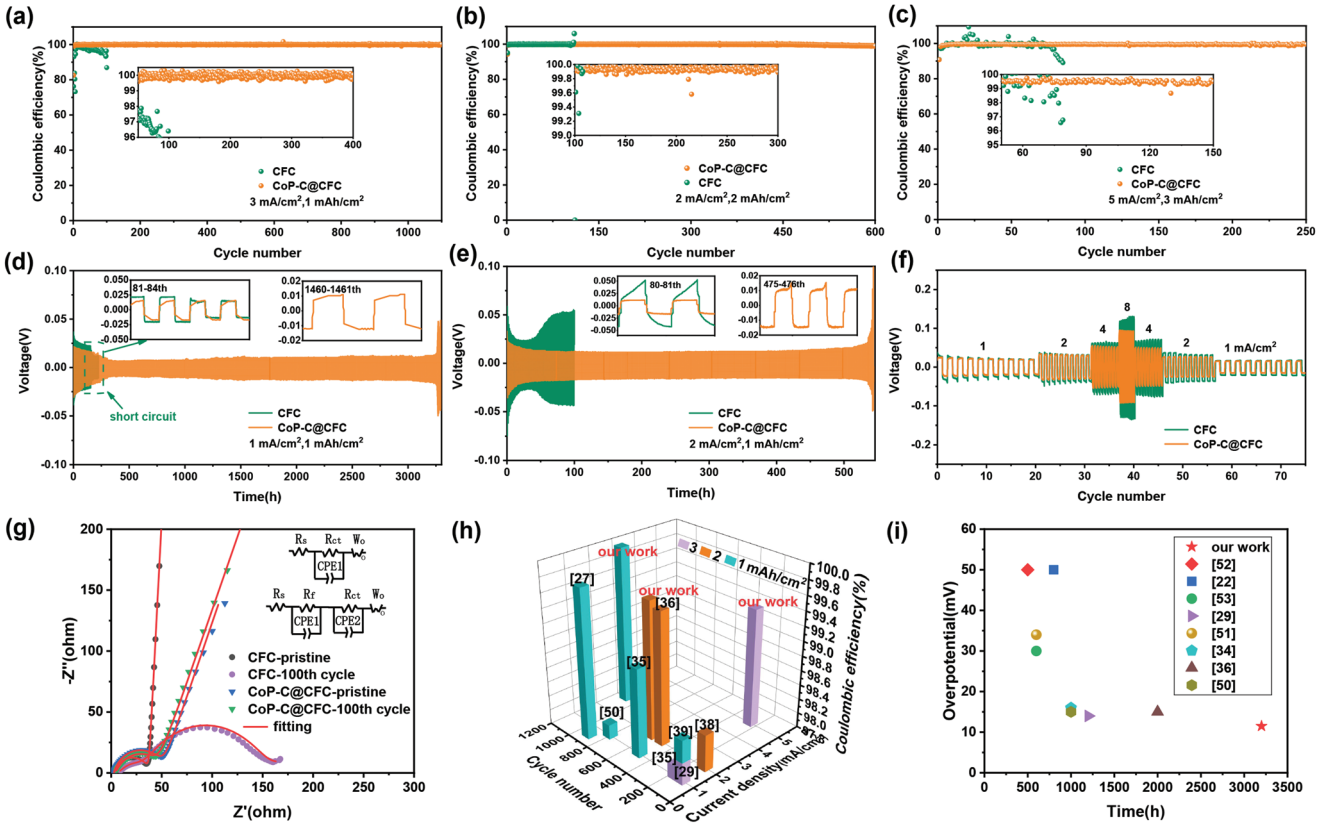

Figure 6. Electrochemical performance of CoP-C@CFC electrodes. a–c) Coulombic efficiency of Li plating/striping on CFC and CoP-C@CFC electrode under different current density and area capacity. d,e) Cycling performance of symmetric cells with CFC-Li and CoP-C@CFC-Li anodes at different test condition. f) Rate performance of symmetric cells with CFC-Li and CoP-C@CFC-Li anodes at various current densities from 1 to 8 mA cm^{-2} with a fixed deposition capacity of 1 mAh cm^{-2}. g) Nyquist plots of CoP-C@CFC-Li anodes at different cycles with their corresponding charge transfer resistance. The performance comparison of h) half cells and i) symmetric cells between CoP-C@CFC and recently reported carbon fiber hosts.

higher current density of 5 mA cm^{-2} with the practical cycling capacity of 3 mAh cm^{-2}, CoP-C@CFC electrode keeps superior average CE of 99.42% over 250 cycles. In voltage–capacity profiles, CoP-C@CFC electrodes (Figure S16, Supporting Information) also exhibit obviously lower polarization voltage and more stable capacity retention than CFC electrodes (Figure S17, Supporting Information). Although the test temperature is increased to 60 °C, the CoP-C@CFC electrode can keep 425 cycles with a high average CE 99.2% at 5 mA cm^{-2} with a total capacity of 3 mAh cm^{-2} (Figure S18g, Supporting Information). Moreover, stable Li plating/stripping can be achieved, which is reflected in voltage–capacity curves (Figure S18h, Supporting Information). Notably, the folding processes of Li||CoP-C@CFC pouch cell with checking the LED illumination further demonstrate the structural stability of the 3D CoP-C@CFC host (Figure S18a–f, Supporting Information). When the CoP-C@CFC electrodes cycle over 50 cycles at 2 mA cm^{-2} with the total capacity of 2 mAh cm^{-2}, the surface of electrode is clean without Li dendrites and the CoP porous sheath still maintains undamaged (Figure S19, Supporting Information), while CFC electrodes show nonuniform Li distribution and much accumulated dead Li (Figure S20, Supporting Information). Comparatively, the half-cell performances of Co_3O_4-C@CFC at 3 mA cm^{-2} with a total capacity of 1 mAh cm^{-2} are shown in Figure S21, Supporting Information, which presents obvious shorter cycle lifespan originated from the formed insulative Li_2O_2 (Figure S22, Supporting Information).[24] Therefore, the high-performance of CoP-C@CFC is attributed to MOF-derived porous carbon sheath with embedded CoP nanoparticles, which uniforms Li^+/electron flux of carbon fiber surface and realizes optimized electrode kinetics.[25] Additionally, symmetric cells are assembled with CoP-C@CFC-Li prestored Li metal of 5 mAh cm^{-2}. As shown in Figure 6d, CoP-C@CFC-Li anode exhibits stable voltage profile with a highly low overpotential of 11.5 mV and ultralong cycling life of 3200 h at 1 mA cm^{-2} with the capacity of 1 mAh cm^{-2} (20% DOD). However, sharp fluctuant voltage over 50 mV and short cycling lifespan less than 100 cycles have been displayed for CFC-Li anode. When the current density of 2 mA cm^{-2} is executed (Figure 6e), the CoP-C@CFC anode can still maintain a stable cycling of about 550 h with a low voltage hysteresis of 13 mV, while the CFC-Li anode displays poor cycling and harsh overpotential. Additionally, excellent rate performance with low voltage polarizations of 15, 30, 50, and 88 mV at 1, 2, 4, and 8 mA cm^{-2}, respectively, could be achieved in Figure 6f. When the current density drops back to 4, 2, and 1 mA cm^{-2}, the voltage polarization still keeps relatively stable values of 47, 26, and 15 mV, respectively. It reveals that the CoP-C@CFC-Li anode exhibits excellent rate capability and high reversibility. By contrast, because of high nucleation barrier alongside with further exacerbated polarization, the

CFC-Li anode displays a larger voltage hysteresis, especially under realistic current density. The interfacial transfer impedance of Li^+ is studied by electrochemical impedance spectroscopy in half cells (Figure 6g).[47,51] At pristine, the CoP-C@CFC-Li and CFC-Li electrodes show a low charge transfer resistance (R_{ct}) of 47.5 and 34.2 Ω, respectively. However, a low charge transfer resistance of 32.2 Ω can be maintained for CoP-C@CFC-Li anode after 100th cycles, while CFC-Li anode shows higher R_{ct} of 109.0 Ω. Meanwhile, the SEI layer of CoP-C@CFC indicates apparent peaks of Li_3P and LiF in high-resolution XPS profiles, while CFC shows strong peaks of Li_2O (Figure S23, Supporting Information). It reveals that superior conductivity and robust SEI layer are probably achieved in the CoP-C@CFC-Li electrodes, which owes to Li_3P@Co interface and stable 3D skeletons. Comparatively, charge transfer resistance continuously increases due to a mass of accumulated dead Li and weak SEI layer on the surface of CFC electrodes. Compared with the most recent reported carbon fiber-based Li host under similar testing conditions, CoP-C@CFC shows the best electrochemical performance with high CE and long cycling lifespan to our knowledge (Figure 6h).[52] Meanwhile, symmetric cells at 20% DOD exhibit lowest overpotential and ultralong cycling time, while most infinite carbon fiber-based Li metal composite anodes have a large overpotential of over 20 mV after 500 h cycling under the same testing conditions (Figure 6i).[53–55]

The potential application of CoP-C@CFC is further explored with full cell, which is assembled with CoP-C@CFC-Li anode and LFP cathode. As shown in **Figure 7**a, CFC-Li‖LFP full-cell exhibits a relatively high capacity at the initial stage, whereas the only reversible capacity of 76 mAh g^{-1} can be remained after 60 cycles at 1 C. By comparison, CoP-C@CFC-Li‖LFP full-cell possesses excellent cycling performance with discharge capacity of 145 mAh g^{-1} and the stable CE of 99.98% over 460 cycles, showing ultrahigh capacity retention of 98.6%. As the charge–discharge rate is enhanced to 2 C (Figure 7b), CoP-C@CFC-Li‖LFP could hold discharge capacity of 130 mAh g^{-1} with a stable CE of 99.92% and a capacity retention of 95.8%. Comparatively, CFC-Li‖LFP shows obvious poorer capacity retention ability with rapid decaying discharge capacity. To further demonstrate the applicability of the CoP-C@CFC, full cells with higher cathode loading of 5 mg cm^{-2} are provided, which still exhibit outstanding long cycling performance at 1 C (Figure S24a, Supporting Information) and 2 C (Figure S24b, Supporting Information). In addition, outstanding rate performance of CoP-C@CFC-Li‖LFP has been achieved in coin cell (Figure 7c). At low rate of 0.2 C, a high reversible capacity of 161 mAh g^{-1} can be realized for CoP-C@CFC-Li anode, while CFC-Li anode merely maintains a discharge capacity of 151 mAh g^{-1}. With the rate increase to 5 C, CoP-C@CFC-Li‖LFP full cell always keeps reversible capacity of 129 mAh g^{-1}. When the rate is restored to 0.5 C, a capacity of 160 mAh g^{-1} is attained again after 100 cycles without appreciable decay. However, CFC-Li‖LFP full cell presents worse reversible capacity and poor rate performance under the same test conditions. Further, the charge/discharge profiles of the two full cells have been exhibited in Figure 7d. The voltage polarization of CoP-C@CFC-Li‖LFP is 293 mV, which is obvious lower than CFC-Li‖LFP (707 mV). In a word, these outstanding performances of full cells indicate MOF-derived porous carbon sheath with embedded CoP nanoparticles can enhance physicochemical property of CFC and obviously improve electrochemical cycling stability.

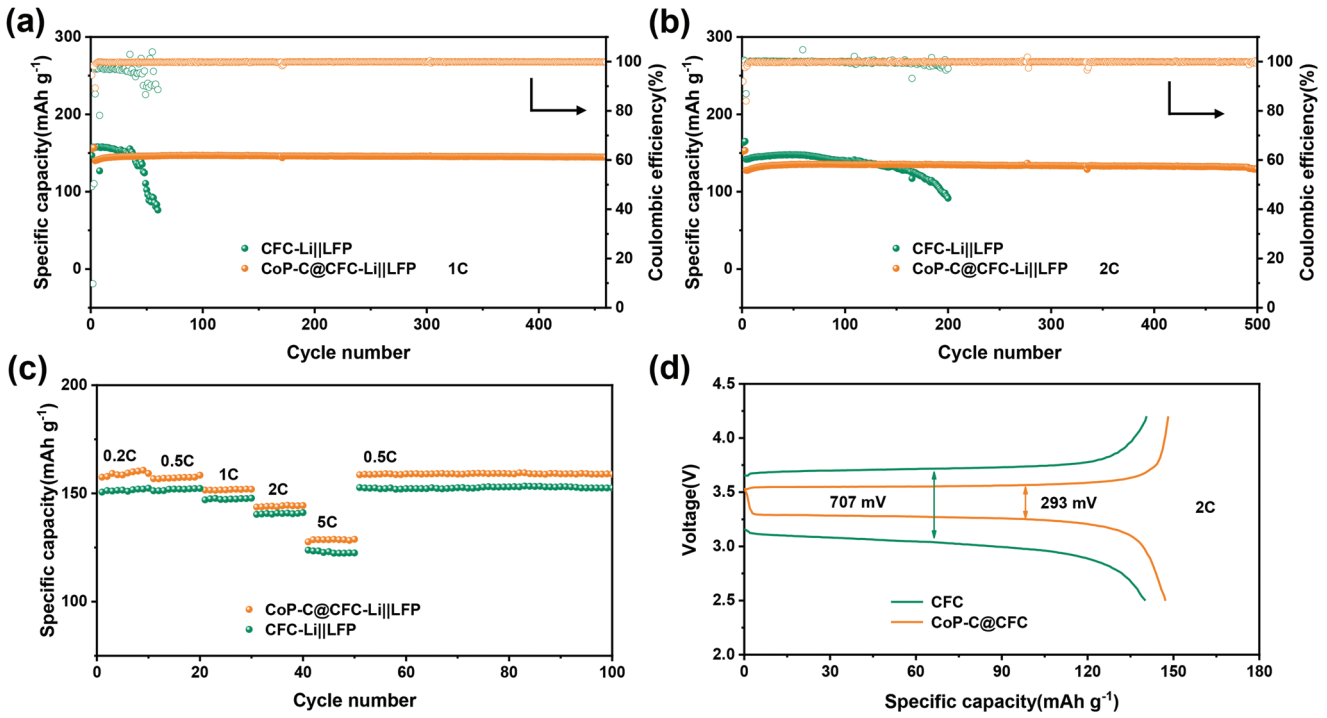

Figure 7. Electrochemical performance of full cells. Cycling performance of CoP-C@CFC-Li‖LFP at a) 1 C and b) 2 C). c) Rate performance of CoP-C@CFC-Li‖LFP. d) The charge/discharge profiles of CoP-C@CFC-Li‖LFP at 2 C.

3. Conclusion

In summary, a 3D mix-conducting matrix decorated with MOF-derived porous carbon sheath with embedded CoP nanoparticles has been well-designed and fabricated by the scalable room-temperature crystallization and annealing-phosphating process. The CoP-C@CFC possesses excellent lithiophilicity and structural characteristics, which effectively increases specific surface area, and highly reduces local current density and nucleation overpotential. In addition, the in situ formed Li_3P@Co lithiophilic interface by the lithiation of CoP-C@CFC provides abundant Li nucleation sites and homogenizes Li-ion flux, which chronically suppresses Li dendrites and volume effect. Thanks to these features, ultralong cycling lifespan of 1100 cycles with outstanding average CE of 99.96% at practical current density of 3 mA cm^{-2} have been achieved. Under higher current density of 5 mA cm^{-2} with the realistic cycling capacity of 3 mAh cm^{-2}, CoP-C@CFC electrode also keeps superior average CE of 99.42% over 250 cycles. And the symmetric battery with finite CoP-C@CFC-Li anode exhibits a low overpotential of 11.5 mV over 3200 h at 1 mA cm^{-2} for 1 mAh cm^{-2} (20% DOD). When the full-cell is assembled with LFP cathode and CoP-C@CFC-Li anode, it displays a capacity retention of 95.8% with 130 mAh g^{-1} over 500 cycles at 2 C and shows excellent rate performance. Importantly, this work lights up MOF-derived metallic phosphide as 3D lithiophilic interface for flexible Li metal anodes.

Supporting Information

Supporting Information is available from the Wiley Online Library or from the author.

Acknowledgements

This work was supported by the National Natural Science Foundation of China (Grant No. 51874361, 52101278, and 52034011) and the Science and Technology program of Hunan Province (2019RS3002 and 2020GK2074).

Conflict of Interest

The authors declare no conflict of interest.

Data Availability Statement

Research data are not shared.

Keywords

cobalt phosphide (CoP) nanoparticles, high reversibility, ion/electron redistribution, lithium metal anodes, metal–organic frameworks

Received: December 10, 2021
Revised: February 25, 2022
Published online: June 24, 2022

[1] F. Li, A. Thevenon, A. Rosas-Hernández, Z. Wang, Y. Li, C. M. Gabardo, A. Ozden, C. T. Dinh, J. Li, Y. Wang, J. P. Edwards, Y. Xu, C. McCallum, L. Tao, Z. Liang, M. Luo, X. Wang, H. Li, C. P. O. Brien, C. Tan, D. Nam, R. Quintero-Bermudez, T. Zhuang, Y. C. Li, Z. Han, R. D. Britt, D. Sinton, T. Agapie, J. C. Peters, E. H. Sargent, *Nature* **2020**, *577*, 509.
[2] Y. Jiao, J. Qin, H. M. K. Sari, D. Li, X. Li, X. Sun, *Energy Storage Mater.* **2021**, *34*, 148.
[3] Y. Zhang, T. Zuo, J. Popovic, K. Lim, Y. Yin, J. Maier, Y. Guo, *Mater. Today* **2020**, *33*, 56.
[4] Y. Liu, Y. Elias, J. Meng, D. Aurbach, R. Zou, D. Xia, Q. Pang, *Joule* **2021**, *5*, 2323.
[5] D. Lin, Y. Liu, Y. Cui, *Nat. Nanotechnol.* **2017**, *12*, 194.
[6] H. Wang, J. He, J. Liu, S. Qi, M. Wu, J. Wen, Y. Chen, Y. Feng, J. Ma, *Adv. Funct. Mater.* **2021**, *31*, 2002578.
[7] W. Wahyudi, V. Ladelta, L. Tsetseris, M. M. Alsabban, X. Guo, E. Yengel, H. Faber, B. Adilbekova, A. Seitkhan, A. H. Emwas, M. N. Hedhili, L. J. Li, V. Tung, N. Hadjichristidis, T. D. Anthopoulos, J. Ming, *Adv. Funct. Mater.* **2021**, *31*, 2101593.
[8] K. Wang, Q. Ren, Z. Gu, C. Duan, J. Wang, F. Zhu, Y. Fu, J. Hao, J. Zhu, L. He, C. Wang, Y. Lu, J. Ma, C. Ma, *Nat. Commun.* **2021**, *12*, 4410.
[9] R. J. Y. Park, C. M. Eschler, C. D. Fincher, A. F. Badel, P. Guan, M. Pharr, B. W. Sheldon, W. C. Carter, V. Viswanathan, Y. Chiang, *Nat. Energy* **2021**, *6*, 314.
[10] Y. Zhu, J. Xie, A. Pei, B. Liu, Y. Wu, D. Lin, J. Li, H. Wang, H. Chen, J. Xu, A. Yang, C. Wu, H. Wang, W. Chen, Y. Cui, *Nat. Commun.* **2019**, *10*, 2067.
[11] C. Niu, H. Lee, S. Chen, Q. Li, J. Du, W. Xu, J. Zhang, M. S. Whittingham, J. Xiao, J. Liu, *Nat. Energy* **2019**, *4*, 551.
[12] T. Mukra, E. Peled, *J. Electrochem. Soc.* **2020**, *167*, 100520.
[13] S. Zhou, I. Usman, Y. Wang, A. Pan, *Energy Storage Mater.* **2021**, *38*, 141.
[14] Z. Liang, K. Yan, G. Zhou, A. Pei, J. Zhao, Y. Sun, J. Xie, Y. Li, F. Shi, Y. Liu, D. Lin, K. Liu, H. Wang, H. Wang, Y. Lu, Y. Cui, *Sci. Adv.* **2019**, *5*, u5655.
[15] J. Pu, J. Li, K. Zhang, T. Zhang, C. Li, H. Ma, J. Zhu, P. V. Braun, J. Lu, H. Zhang, *Nat. Commun.* **2019**, *10*, 1896.
[16] Y. Cheng, X. Ke, Y. Chen, X. Huang, Z. Shi, Z. Guo, *Nano Energy* **2019**, *63*, 103854.
[17] Y. Cheng, J. Chen, Y. Chen, X. Ke, J. Li, Y. Yang, Z. Shi, *Energy Storage Mater.* **2021**, *38*, 276.
[18] S. Fang, L. Shen, A. Hoefling, Y. Wang, G. Kim, P. A. van Aken, X. Zhang, S. Passerini, *Nano Energy* **2021**, *89*, 106421.
[19] H. Kwon, J. Lee, Y. Roh, J. Baek, D. J. Shin, J. K. Yoon, H. J. Ha, J. Y. Kim, H. Kim, *Nat. Commun.* **2021**, *12*, 5537.
[20] H. Chen, Y. Yang, D. T. Boyle, Y. K. Jeong, R. Xu, L. S. de Vasconcelos, Z. Huang, H. Wang, H. Wang, W. Huang, H. Li, J. Wang, H. Gu, R. Matsumoto, K. Motohashi, Y. Nakayama, K. Zhao, Y. Cui, *Nat. Energy* **2021**, *6*, 790.
[21] W. Ye, L. Wang, Y. Yin, X. Fan, Y. Cheng, H. Gao, H. Zhang, Q. Zhang, G. Luo, M. Wang, *ACS Energy Lett.* **2021**, *6*, 2145.
[22] S. Li, Q. Liu, J. Zhou, T. Pan, L. Gao, W. Zhang, L. Fan, Y. Lu, *Adv. Funct. Mater.* **2019**, *29*, 1808847.
[23] X. Yan, L. Lin, Q. Chen, Q. Xie, B. Qu, L. Wang, D. L. Peng, *Carbon Energy* **2021**, *3*, 303.
[24] C. Sun, A. Lin, W. Li, J. Jin, Y. Sun, J. Yang, Z. Wen, *Adv. Energy Mater.* **2019**, *10*, 1902989.
[25] Z. Luo, S. Li, L. Yang, Y. Tian, L. Xu, G. Zou, H. Hou, W. Wei, L. Chen, X. Ji, *Nano Energy* **2021**, *87*, 106212.
[26] B. Hong, H. Fan, X. Cheng, X. Yan, S. Hong, Q. Dong, C. Gao, Z. Zhang, Y. Lai, Q. Zhang, *Energy Storage Mater.* **2019**, *16*, 259.
[27] T. Yang, T. Qian, X. Shen, M. Wang, S. Liu, J. Zhong, C. Yan, F. Rosei, *J. Mater. Chem. A* **2019**, *7*, 14496.

[28] W. Zeng, X. Zhang, C. Yang, C. Zhang, H. Shi, J. Hu, Y. Zhao, W. Zhang, G. Zhang, H. Duan, *Chem. Eng. J.* **2021**, *412*, 128661.
[29] Y. Lu, J. Wang, Y. Chen, X. Zheng, H. Yao, S. Mathur, Z. Hong, *Adv. Funct. Mater.* **2021**, *31*, 2009605.
[30] S. Liu, X. Xia, Z. Yao, J. Wu, L. Zhang, S. Deng, C. Zhou, S. Shen, X. Wang, J. Tu, *Small Methods* **2018**, *2*, 1800035.
[31] S. Ye, F. Liu, R. Xu, Y. Yao, X. Zhou, Y. Feng, X. Cheng, Y. Yu, *Small* **2019**, *15*, 1903725.
[32] Y. Mei, J. Zhou, Y. Hao, X. Hu, J. Lin, Y. Huang, L. Li, C. Feng, F. Wu, R. Chen, *Adv. Funct. Mater.* **2021**, *31*, 2106676.
[33] H. Shen, F. Qi, H. Li, P. Tang, X. Gao, S. Yang, Z. Hu, Z. Li, J. Tan, S. Bai, F. Li, *Adv. Funct. Mater.* **2021**, *31*, 2103309.
[34] J. Zhu, J. Chen, Y. Luo, S. Sun, L. Qin, H. Xu, P. Zhang, W. Zhang, W. Tian, Z. Sun, *Energy Storage Mater.* **2019**, *23*, 539.
[35] M. Zhu, J. Zhang, Y. Ma, Y. Nan, S. Li, *Carbon* **2020**, *168*, 633.
[36] Y. Fang, W. Cai, S. Zhu, K. Xu, M. Zhu, G. Xiao, Y. Zhu, *J. Energy Chem.* **2021**, *54*, 105.
[37] T. S. Wang, X. Liu, Y. Wang, L. Z. Fan, *Adv. Funct. Mater.* **2021**, *31*, 2001973.
[38] T. Zhou, J. Shen, Z. Wang, J. Liu, R. Hu, L. Ouyang, Y. Feng, H. Liu, Y. Yu, M. Zhu, *Adv. Funct. Mater.* **2020**, *30*, 1909159.
[39] G. Jiang, N. Jiang, N. Zheng, X. Chen, J. Mao, G. Ding, Y. Li, F. Sun, Y. Li, *Energy Storage Mater.* **2019**, *23*, 181.
[40] L. Chen, G. Chen, W. Tang, H. Wang, F. Chen, X. Liu, R. Ma, *Mater. Today Energy* **2020**, *18*, 100520.
[41] D. Liang, H. Jiang, Q. Xu, J. Luo, Y. Hu, C. Li, *J. Electrochem. Soc.* **2018**, *165*, F1286.
[42] Z. Wang, J. Shen, J. Liu, X. Xu, Z. Liu, R. Hu, L. Yang, Y. Feng, J. Liu, Z. Shi, L. Ouyang, Y. Yu, M. Zhu, *Adv. Mater.* **2019**, *31*, 1902228.
[43] H. Su, Y. Zhang, X. Liu, F. Fu, J. Ma, K. Li, W. Zhang, J. Zhang, D. Li, *J. Colloid Interface Sci.* **2021**, *582*, 969.
[44] D. Liu, W. Lu, K. Wang, G. Du, A. M. Asiri, Q. Lu, X. Sun, *Nanotechnology* **2016**, *27*, 42.
[45] H. Jiang, H. Fan, Z. Han, B. Hong, F. Wu, K. Zhang, Z. Zhang, J. Fang, Y. Lai, *J. Energy Chem.* **2021**, *54*, 301.
[46] N. Wu, Y. Li, A. Dolocan, W. Li, H. Xu, B. Xu, N. S. Grundish, Z. Cui, H. Jin, J. B. Goodenough, *Adv. Funct. Mater.* **2020**, *30*, 2000831.
[47] H. Jiang, Y. Zhou, H. Zhu, F. Qin, Z. Han, M. Bai, J. Yang, J. Li, B. Hong, Y. Lai, *Chem. Eng. J.* **2022**, *428*, 132648.
[48] Z. Liu, S. Yang, B. Sun, X. Chang, J. Zheng, X. Li, *Angew. Chem., Int. Ed. Engl.* **2018**, *57*, 10187.
[49] K. Guo, B. Xi, R. Wei, H. Li, J. Feng, S. Xiong, *Adv. Energy Mater.* **2020**, *10*, 1902913.
[50] L. Gao, J. Li, B. Sarmad, B. Cheng, W. Kang, N. Deng, *Nanoscale* **2020**, *12*, 14279.
[51] J. Wang, W. Huang, A. Pei, Y. Li, F. Shi, X. Yu, Y. Cui, *Nat. Energy* **2019**, *4*, 664.
[52] Y. Fang, S. L. Zhang, Z. Wu, D. Luan, X. W. D. Lou, *Sci. Adv.* **2021**, *7*, g3626.
[53] P. Zhang, C. Peng, X. Liu, F. Dong, H. Xu, J. Yang, S. Zheng, *ACS Appl. Mater. Interfaces* **2019**, *11*, 44325.
[54] B. Liu, Y. Zhang, G. Pan, C. Ai, S. Deng, S. Liu, Q. Liu, X. Wang, X. Xia, J. Tu, *J. Mater. Chem. A* **2019**, *7*, 21794.
[55] L. Tao, A. Hu, Z. Yang, Z. Xu, C. E. Wall, A. R. Esker, Z. Zheng, F. Lin, *Adv. Funct. Mater.* **2020**, *30*, 2000585.